Frequency resolved optical gating for ultrashort mid-infrared laser pulses

Luís de Gonzaga Ferin de Melo da Cunha Veloso
luis.veloso@tecnico.ulisboa.pt

Instituto Superior Técnico, Lisboa, Portugal

October 2021

Abstract

The broadening set of applications of ultrashort laser pulses has driven researchers in the past decades to continuously push through to obtain shorter and shorter pulses. One shortcoming of this are the challenges in their measurement if there is no other shorter pulse available to compare it with. The FROG technique, first presented in 1991, is capable of characterizing these pulses. But the development in the past decade of ultrashort pulses in the mid-infrared raises new challenges in their measurement due to the inherent difficulties in the manipulation of beams in said wavelength range. In this work, we develop a FROG diagnostic for ultrashort pulses in the mid-infrared. In particular, we benchmark and use a state of the art ptychography based algorithm against a traditional one to achieve superior precision in complex pulses. To tackle the difficulties of the mid-infrared region in the SHG process, we use a $AgGaS_2$ crystal. We thus characterize two 1 µm laser pulses, an oscillator and a high power one using FROG, and a 3 µm OPCPA laser pulse using the autocorrelation method. Knowing the pulse length is the foundation on which future research in optics in this laboratory is built.
Keywords: Mid-infrared, ultrashort, laser, FROG, SHG, ptychography

1. Introduction

Ever since their invention in 1960, lasers have found applications in numerous fields, ranging from research, to everyday use, from the detection of gravitational waves, to DVD players. Indeed, in addition to the multiple laser related Nobel prizes, more than fifty-five thousand patents involving the laser have been granted in the United States alone, averaging at about three per day [1]. Driven by the broadening set of applications made available by their existence, researchers are continuously pushing through to obtain shorter and shorter laser pulses. From the probing of ultrafast physical, chemical and biological processes [1], to ultrafast optical fiber communications, ultrashort laser pulses progressively unlock new possibilities. However, it is of little use to strive for ever shorter laser pulses if we are not able to measure them. This measurement goes beyond the issue of temporal length alone, but also involves the pulse structure and phase.

1.1. Objectives and methods

The emergence of ultrashort laser pulses in the range of only a few femtoseconds (10^{-15} s) has brought a number of new challenges to this field. To measure a certain event, we must use shorter ones; for instance, a stopwatch is used to measure the speed of an athlete, a camera with a fast shutter to capture a bird flapping its wings... But how can we measure the shortest events ever created? There is no shorter event to compare it with. We somehow have to make do with the second best thing: the pulse itself.

Manipulating ultrashort pulses also has its difficulties. Most noteworthy of all is that extremely large bandwidths have to be handled, from tens to hundreds of nm. Indeed, to process an ultrashort pulse, special attention must be paid to the choice of materials used in the optical system to ensure that they can accommodate the desired optical processes without losses, distortions or excessive dispersion. For instance, in this work, the Frequency-Resolved Optical Gating (FROG) technique mixes two signals in a non-linear medium to form a third one, be it through second - or third - harmonic generation, a polarization gate, etc... Regardless, the materials should be able to carry out their intended purpose, as best as possible, without altering the pulse itself or distorting the desired information.

The past decade has witnessed the emergence in particular of ultrashort laser systems in the mid-infrared spectral range (2-10 µm). In this region, the above listed problems become even more evi-

[1] LaserFest — Early History.

dent due to the lack of suitable equipment and the bandwidth being even broader. Note that, for a 100 fs pulse, the bandwidth (in wavelength range) is around 20 times larger at 3000 nm than at 650 nm. The materials must then be validated for operation in the full wavelength range of our laser pulses.

Given the expensive cost of FROG devices, particularly in the mid-infrared, and the fact that the host research group has the necessary know-how and equipment, it was decided to design, build, test and demonstrate this device using our own resources, which is the main content of the work described in this thesis. The ultimate goal to achieve with this work is full temporal characterization of the laser pulses of the novel 3 µm OPCPA (Optical parametric chirped-pulse amplification) Fastlite laser system laser system.

1.2. State of the art

When we talk about measuring a pulse, we actually mean determining its electric field as a function of time and/or space. Assuming that the spatial and temporal quantities are independent we can write the (real) electric field as a function of time as:

$$\mathcal{E}(t) = \frac{1}{2}\sqrt{I(t)}\exp\{i[\omega_0 t - \phi(t)]\} + c.c., \qquad (1)$$

where t is the time in the reference frame of the pulse, ω_0 is a carrier angular frequency, and $I(t)$ and $\phi(t)$ are the pulse intensity and temporal phase. The complex conjugate (c.c.) is necessary to make the pulse real, but can be ignored to simplify the calculations and added back at any time. Usually, we wish to obtain the pulse complex amplitude:

$$E(t) = \sqrt{I(t)}\exp[-i\phi(t)] \qquad (2)$$

Fourier transforming this to the frequency domain, we have:

$$\widetilde{E}(\omega) = \sqrt{S(\omega)}\exp[-i\varphi(\omega)] \qquad (3)$$

where $S(\omega)$ is the spectral intensity (also called "the spectrum") and $\varphi(\omega)$ is the spectral phase. And so, the pulse duration that we are looking for is actually the FWHM of the temporal intensity, $I(t)$.

In terms of pulse lengths, it is common practice to classify as "ultrashort" those pulses not exceeding a few hundreds of femtoseconds, although this limit has become shorter over the years.

The spectrum $S(\omega)$ has been the most straightforward of these quantities to obtain. However, to fully characterize a pulse, it is necessary to have the intensity and the phase in any of the two domains (time or frequency). This problem is called the one-dimensional phase-retrieval problem. As it turns out, we do not have enough constraints to uniquely determine the phase. There are, for starters, the

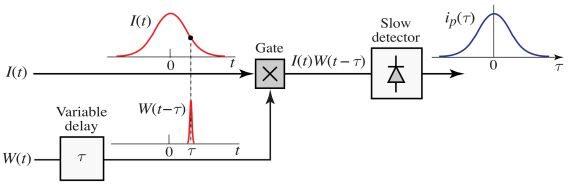

Figure 1: Schematic of the concept behind the technique for measuring an optical pulse by use of an optical gate [1, p. 1147]. The gating function $W(t)$ is delayed and then operates the gate to retrieve, with the detector, the portion corresponding to that delay of the initial pulse $I(t)$. Repeating the measurement for all portions of the initial pulse allows to reconstruct the pulse.

"trivial" ambiguities. If we have a certain spectrum for a pulse of electric field $E(t)$, adding a constant phase shift $E(t)\exp(i\phi_0)$ will not change its spectrum. The same goes for a time translation $E(t-t_0)$, and a time reversal $E^*(-t)$. But besides these ambiguities, there are other much more problematic ones [2, 3].

The first technique developed to measure laser pulses dates back to the 1960's. To measure a continuous quantity in two dimensions, several discrete measurements have to be made to trace an approximate profile of the function. The shorter the interval between those measurements, the more precise is the trace. In optics, this is done using a gating function (or signal), where the measurement is made during a short time interval. By repeating this measurement in all the portions of the pulse, we obtain a signal that is proportional to the area under the transmitted pulse. Now, to operate this gate, electronic devices are too slow, so a shorter laser pulse plays the role of the gate. This gating phenomenon can be achieved e.g. by using a pulse mixing nonlinear process such as second harmonic generation. The two pulses are overlapped in a nonlinear medium, creating a third pulse that is then detected by the camera. Imparting a controllable delay on to the gating pulse will allow obtaining the range of measurements necessary to reconstruct the pulse that we wish to obtain.

We now face the problem that no shorter pulse is available for our gating function. In this case the pulse is used to gate itself. The photocurrent measured will then be proportional to the intensity autocorrelation:

$$A^{(2)}(\tau) = \int_{-\infty}^{\infty} I(t)I(t-\tau)\,dt. \qquad (4)$$

From this, we can obtain the magnitude of the quantity that we want, $I(t)$, but we are lacking the phase. We are facing here again the one di-

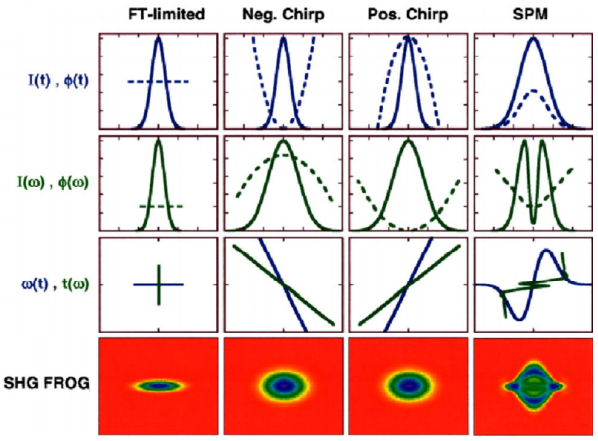

Figure 2: FROG traces for common ultrashort-pulse distortions [5, p. 55-56]. Each column shows a different pulse example. The first line shows the time dependent intensity and phase for a given pulse; the second, the frequency dependent intensity and phase; the third, the phase vs time and time vs phase; the final line represents the spectrogram.

mensional phase-retrieval problem. Yet, this technique allowed for rough estimations of pulse length. However, it involves making a guess as to the pulse shape. We can then derive analytically a multiplicative factor relating the intensity to the full-width-half-maximum of the autocorrelation.

In 1991 [4] a new approach was considered, consisting in obtaining a frequency resolved autocorrelation, i.e. measuring the delay-dependent pulse spectrum rather than just its intensity. This results in a new domain of operation: the time-frequency domain. The mathematical description of this is the spectrogram (a.k.a. "trace"):

$$\Sigma_g(\omega,\tau) = \left| \int_{-\infty}^{\infty} E(t) g(t-\tau) exp(-i\omega t)\, dt \right|^2 \quad (5)$$

This is the Fourier transform of a gated pulse, where $g(t-\tau)$ is a gate function with variable delay; the spectrogram is then a two-dimensional representation of the wave form as a function of the frequency and the delay. Figure 2 shows some examples of spectrogram traces. This is called the frequency resolved optical gating (FROG) technique. A useful characteristic of this trace is that we can still recover the information of the autocorrelation by simply integrating the signal in frequency. However, we now face the two-dimensional phase-retrieval problem, but, surprisingly, by complicating the problem, it can now be solved, thus yielding a unique solution for the pulse. Only the trivial ambiguities persist.

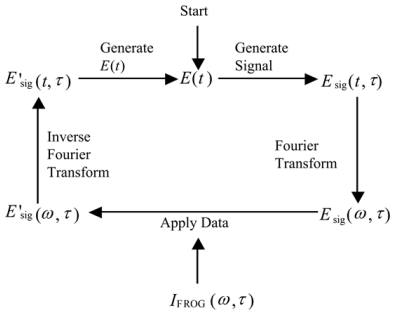

Figure 3: FROG generic algorithm [5, p. 71].

To recover the actual pulse length form the trace, we need a FROG algorithm. This kind of algorithm is an iterative one and there are many different versions. In a generic FROG algorithm (Fig. 3) the starting point is making an initial guess for the E-field $E(t)$. A signal of the field $E_{sig}(t,\tau)$ is generated, which is then Fourier transformed to obtain the spectrogram $E_{sig}(\omega,\tau)$. At this point the measured trace is compared with our field in the spectral domain. The trace in the time-frequency domain is then used to improve the estimation. This is done by comparing and adjusting the magnitudes of $|E_{sig}(\omega,\tau)|^2$ as it should be equal to $I_{FROG}(\omega,\tau)$. This corrected field is then inverse transformed back into the time domain. Finally, a new guess for the electric field is generated to repeat the process. Ideally, each new guess is better than the previous one and the method converges into the true field.

In 2016, a new method based on ptychography was introduced [6]. It outperformed previous algorithms in terms of robustness to noise and speed. It operates as a regular FROG algorithm but it introduces a loop within the pre-existent loop, and corrects each spectrum line in a random order, instead of making a correction on the full trace. Essentially, it works in 1D instead of 2D.

In 2010, P. K. Bates, presented the first full description of a FROG characterization device for mid-IR pulses [7].

2. Design and dimensioning of the FROG diagnostic

For reference, figure 4 shows a standard SHG-FROG diagram. The beams start by being split in two from the original one in the beamsplitter. One of them suffers a delay before both being recombined in the crystal. Among the available methods of combining beams, we chose the second harmonic generation one. SHG-FROG is suitable for few-cycle pulses [8] [9] and is the most popular among these techniques because it introduces little material dispersion before the non-linear process occurs [10]. Moreover, SHG FROG achieves the

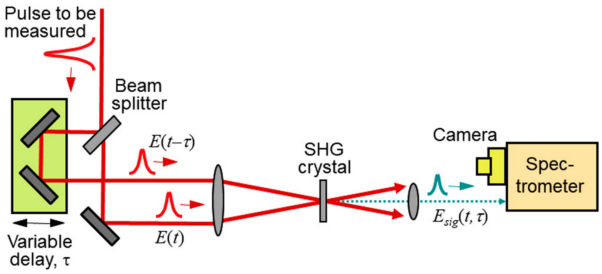

Figure 4: SHG-FROG diagnostic diagram [11, p. 14]. The initial beam is split in two in the beamsplitter. One of the beams is delayed, before recombining both in the SHG-crystal. The detector captures the spectrum corresponding to that delay.

best signal-to-noise ratios because it is the strongest (lowest order) non-linearity and its signal beam is a different wavelength, so scattered light is easily filtered. [11]

2.1. Design requirements

Taking into account the already discussed characteristics of the laser pulses, in particular their ultrashort duration, we know that dispersion is likely to be an issue. We will then preferably use components that are not transmitters, but rather reflective to prevent any material dispersion to take place. Another issue is the pulse bandwidth. This means that we will have to use components suited to these characteristics to ensure that the spectrum is not cut anywhere. In the case where there is no alternative to a transmitter component, then we will look to achieve a minimal width of said component in order to reduce its dispersion effect. Such is the case of, for one, the beamsplitter.

A more practical requirements is to automate the delay generation. If we manually displaced the moving surface on top of which are positioned the mirrors introducing the delay, besides being less precise, each acquisition would drag on for a long time, which would also increase the chances of incoherent readings as the changes in the conditions of the experiment are more likely to be noticeable.

2.2. Components

As with every optics practical work, we will need mirrors to direct the beams as we want them, as well as irises for their alignment. Considering what we have discussed in the previous section, we should look into the coating options. Protected silver mirrors were elected due to their high reflectance properties in the mid-infrared. In this wavelength range, these mirrors have an average reflection above 97% in the infrared region [2].

[2]Metallic Mirrors — Protected Gold, Silver, Aluminium Mirrors — EKSMA Optics.

As commented, we would prefer reflecting components instead of transmitting ones, and so, we opted for a parabolic mirror to focus the two beams in the crystal. This mirror is also coated with silver.

For the beamsplitter, we opted for a zinc selenide (ZnSe) due to its suitable transmission and reflection properties in the mid-infrared; at 3 µm we have around 55% reflection and 45 % transmission.

For the collimating lens we chose a CaF_2 spherical one. Since after the nonlinear crystal we have the desired mixing signal, the pulse duration after this point is no longer important so dispersion is not a major concern.

To solve the moving surface automation issue, we chose to use a translation motor acting on a linear translation stage. This motor would then need to be programmed, in parallel with the spectrometer so that they can work in sync and the diagnostic be fully automated.

2.3. The SHG crystal

A component that plays a key part in the setup is the crystal that fuses the two beams. We were looking for a crystal with a wide bandwidth and a great conversion efficiency. As no process in the diagnostic would alter the polarization of one of the beams, we also needed the phase matching to occur in same polarization. To compare the crystals, we used SNLO.

Given the criteria, several crystals were suitable candidates, but of all, only the $AgGaS_2$ crystal is readily available, and while it is not the one with the largest bandwidth, it is the one used by P. K. Bates [7], so that's the one we opted for. The interaction type was a type I phase matching. At 3 µm the transmission is around 0.7. Regarding the conversion efficiency, while comparing with other crystals, we see that the power conversion efficiency can be 100 times higher. However, we are already ensured by P. K. Bates' work that it is adapted to this application, and we were very confident on the power of our laser (≈4.5W). We opted for a thickness of 100 nm which resulted in a bandwidth of 3250 nm, which is amply sufficient (about 8 times larger than what we need) to ensure there are no cuts in the spectrum.

Given everything, the final design is shown in figure 5. Notice that there are four more mirrors than strictly necessary in the entry and exit point. This is standard procedure in optics, in order to have control over how the beam enters and exits the setup.

2.4. Retrieval algorithm: traditional vs. ptychographic

A final aspect we looked into before proceeding was how this ptychographic algorithm fared against others, and in particular against one that we al-

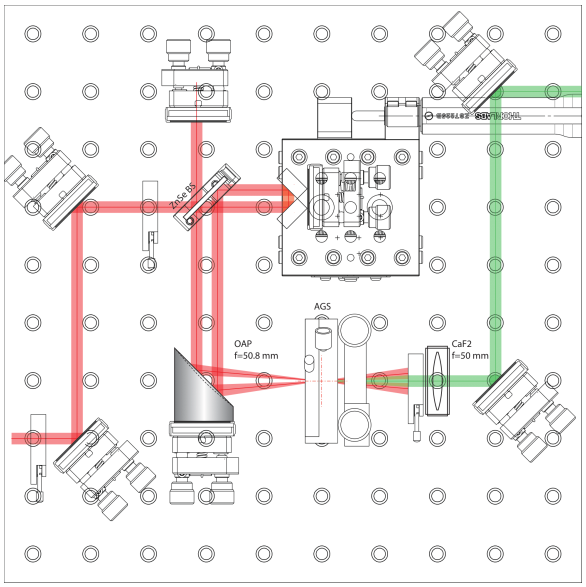

Figure 5: Design of our SHG-FROG. From the entry point on the left, the beam goes through an iris two mirrors, and another iris. The beamsplitter splits the beam. One part is reflected back in a mirror, the other in the retroreflector on top of the linear translation stage. Both beams move on to the concave mirror and to the crystal. A lens with an iris mounted on it collimates the beam. Two mirrors redirect the beam to the exit.

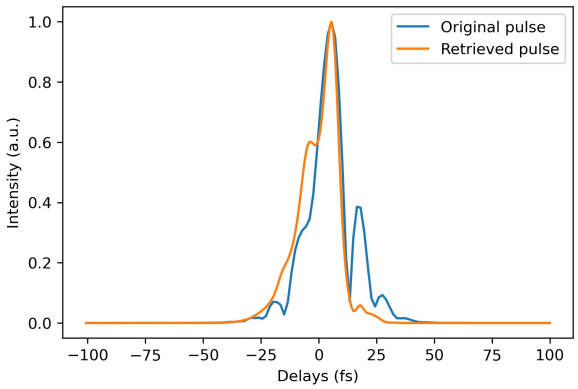

Figure 6: Comparison of the retrieved and original test pulse using Femtosoft

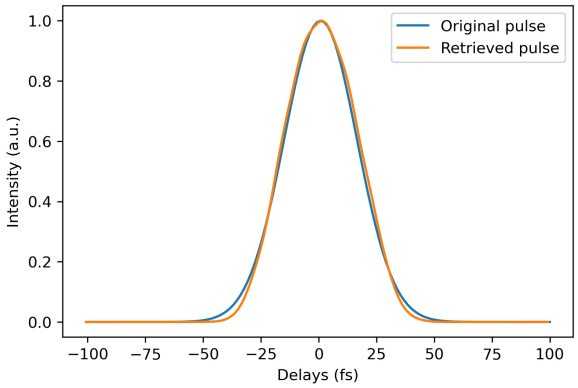

Figure 7: Comparison of the retrieved and original Gaussian pulse using Femtosoft

ready had in the laboratory. This was a software called Femtosoft published by Rich Trebino through "Swamp Optics" that has been discontinued. The code of the ptychographic algorithm had a pulse bank from which we could choose one and test the code. The recovery was nearly perfect with an error of 0.009. We then ran the same pulse through our older program. Figure 6 shows the retrieved and original pulses. The error reported by the software is about double that of the ptychographic one, but still very low, at 0.017, although visually, the retrieval is way off, which raises concerns as to that number's reliability. Indeed, the ptychographic algorithm does provide much more confidence as to its precision, and this benchmark attests to its robustness to noise in comparison with others. Nevertheless, the pulses that we would be characterizing are less nuanced than this test pulse. They would be more Gaussian-like and thus, easier to recover. To make sure of that we created a Gaussian pulse with only a real part and ran it through both algorithms again. The ptychografic algorithm retrieved the pulse perfectly again, although it maintained an error of 0.01, and the Femtosoft software did indeed produce satisfactory results regarding the intensity with an error of 0.005 as shown in figure 7. However, the phase was not zero as it should be for an ideal pulse with no imaginary part. We can then rely on this software for simple pulses, but have to be doubtful as to its retrieved phase.

3. Alignment and operation of the FROG apparatus

Besides the actual diagnostic, there were two other main elements that had to be put together. The motor programming and the spectrum acquisition, both in LabVIEW. These two worked in essentially two separate blocks.

3.1. Step motor configuration

The FROG trace is essentially the spectrum of the fused beam for multiple even delays of the deviated beam. With ultrashort pulses, the space intervals we need between measurements are in the order of the µm.

To program the motor, we used the software LabVIEW, a systems engineering software for applications that require test, measurement, and control with rapid access to hardware and data insights. What we essentially wanted to obtain, is a control frame where we would input our time interval and

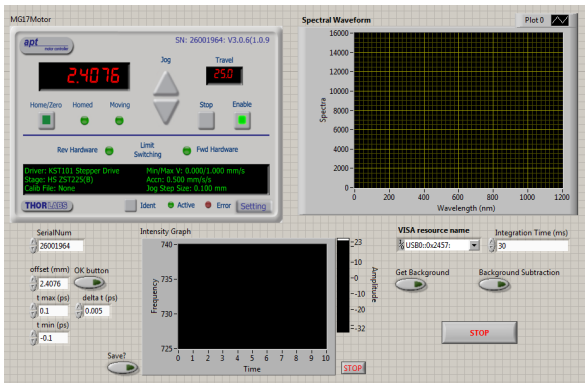

Figure 8: LabVIEW FROG front panel. Up-left: Motor widget. Up-right: Spectrometer widget. Down: Spectrogram widget

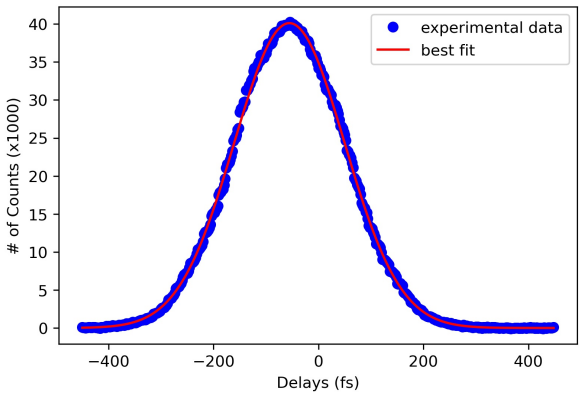

Figure 9: Gaussian fit of the oscillator autocorrelation

the delay interval and have the motor go through that range. A series of calculations converted the space displacement into a time delay. The communication with the motor was then established to actually move the motor.

3.2. Measurement interface

Now that we were able to obtain the delays, we only needed to obtain the spectrum for each of them. Again, instead of manually obtaining them, the process was automated using LabVIEW. This allowed to articulate the spectrometer with the motor, so that after entering the initial parameters, the program ran the acquisition in one go, retrieving the spectrum for each delay and printing the final result in a data file, ready to be analysed. In addition to that, our LabVIEW interface presented a series of widgets that allowed to easily control the parameters and see the results. Figure 8 shows the front panel of the program.

Not everything goes as planned, and in our available time frame, we had not the opportunity to integrate the 3 µm spectrometer into our LabView program. So, instead of actually retrieving a FROG trace, we would now obtain the autocorrelation since we had a suitable photodiode, and knew how to use it. Although less precisely, we would still accomplish what we set out to do; to characterize an ultrashort mid-infrared pulse.

For that purpose, we devised a similar LabVIEW program. Instead of the live spectrum, it now retrieves the live intensity and shows the final autocorrelation.

4. Experimental results and discussion

Two trial runs were executed first using two 1 µm lasers whose pulses we already knew. For both of these, we obtained and analysed the autocorrelation and then applied both FROG algorithms. Finally, we obtained the autocorrelation of the final 3 µm.

4.1. Coherent Mira Ti:sapphire oscillator

The first laser we characterized is a coherent Mira Ti:sapphire oscillator. It operates at repetition rate of 76 MHz, with pulse energy of the order of the nJ and wavelength of 1032 nm. The pulse length is of the order of 100 fs. We scanned the delay stage in steps of 2 fs, over a range of 900 fs, corresponding to 450 points of delay with a step size of 0.3 µm.

We obtained the autocorrelation by integrating the FROG trace in frequency. We have to make a guess regarding the pulse shape in order to estimate its width. Given the simple spot-like spectrogram retrieved (Fig. 12) we assumed a Gaussian shape (a sech^2 could also have been appropriate), and applied its form factor to yield the approximated pulse width. Figure 9 shows the autocorrelation and the Gaussian function that best fits the data. The FWHM of the curve is of 248 fs, and thus, the pulse width is of around $248/1.414 = 174$ fs. It fits in the order of magnitude we anticipated.

However, to check if this pulse width was physically possible we proceeded with a simple test. Equation 4.1 gives a relation between the wavelength peak λ, the bandwidth $\Delta\lambda$ and the pulse width $\Delta\tau$, and a quantity called the time bandwidth product, TBWP.

$$\Delta\tau \cdot \Delta\lambda \cdot \frac{c}{\lambda^2} = TBWP \tag{6}$$

For each pulse shape, there is a minimum TBWP possible. If the pulse width that we found previously resulted shorter than the minimum pulse width calculated with equation 4.1 by plugging in the minimum TBWP possible, then our measurement had to be incorrect. Assuming a Gaussian pulse, the minimum TBWP is 0.44, and the calculation reports a minimum pulse width of 128 fs which is indeed largely inferior to the 174 fs measured. This is a reassurance that the pulse is indeed possible.

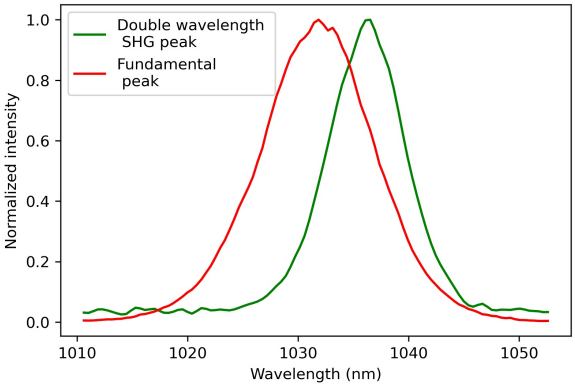

Figure 10: Plot of the oscillator spectrum of the fundamental pulse and of the second harmonic with its wavelength axis doubled.

We also ran a test to verify that the result was credible. It consisted in doubling the wavelength of each point of the spectrum of the second harmonic and compare it with the spectrum of the fundamental peak of the beam (the one coming directly from the laser). Again, the spectrum was obtained by integrating the FROG traces, but in this instance, in time. Figure 10 shows both spectra.

This test would serve two purposes. The first, to ensure that it was indeed the second harmonic that we were obtaining. The second, to check if there were any cuts in frequency. Theoretically, the two curves should overlap perfectly. This remains a mostly qualitative test, and so the results were deemed satisfactory despite the minor differences explained by the not perfect linearity of the spectrometer.

We now ran the trace through Femtsosoft. Figure 12 shows the visual comparison between the original and retrieved traces. Figure 11 shows the retrieved electric field. A pulse width of 188.2 fs is retrieved with an error 0.001, however, this error does not correspond to the error of the pulse of this full technique, as it does not take into account the errors in retrieving the trace.

Regarding the phase, we notice that the pulse has some linear chirp due to its parabolic phase, although, we cannot be sure of this due to the uncertainty created with the benchmark. A chirped signal has its frequency changing with time.

The error reported is very tiny. As commented in section 2, we need to be wary of this value. What it can be useful for is to compare it with the error of the test characterization. The error then was of 0.017, which is 18 times larger than this one. As expected, this software effectively retrieves simpler pulses such as this one, so we can be more confident in its result than in our first benchmark

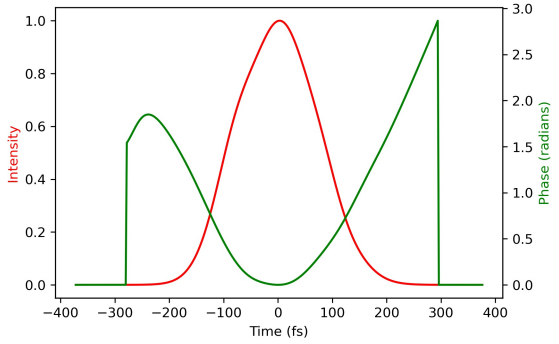

Figure 11: Retrieved oscillator pulse and phase using Femtosoft

pulse in section 2.

We finally ran the pulse through the ptychographic algorithm. Figure 12 shows the original and retrieved traces. We can see the retrieval was mostly successful.

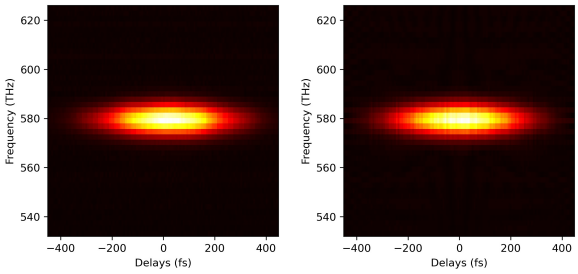

Figure 12: Original (left) and retrieved (right) FROG oscillator traces using the ptychographic algorithm

The error reported is of 0.084. This large error can be explained by the squeezed format we had to input the data in. Indeed, the algorithm requires the data to be plugged in with the product $dt \cdot dF = 1/N$, where dt is the delay interval between pixels, dF the frequency difference between pixels, and N the grid size, i.e. number of pixels in an axis. We thus cannot stretch interpolating the data in wavelengths more to have more points. We would need a spectrometer with higher resolution for more precise results.

Fitting a Gaussian in the retrieved temporal pulse data (Fig. 13) yields a pulse width of 201 fs. Of course, we are assuming that the pulse is Gaussian-like, but this assumption does seem accurate, looking at the figure. This retrieval differs by 12.8 fs from Femtosoft. We have already talked about Femtosoft's efficacy in retrieving simple pulses, so, given the previous one presented an error 10 times smaller, we are more confident that 188.2 fs is the true value. Also, an 8.4% error in

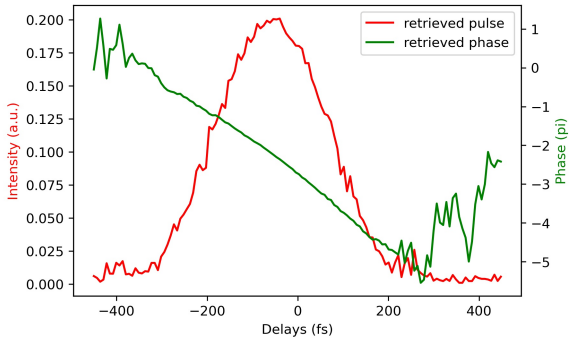

Figure 13: Ptychographic recovery of the oscillator pulse and phase

201 fs represents the interval [184 ; 218] fs, which includes the Femtosoft's 188.2 fs result.

Regarding the phase, we can now see that this pulse has no chirp due to the linear phase rather than the linear chirp with the previous algorithm. Given the benchmark in section 2, we deem this one to be more trustworthy.

4.2. Amphos Yb:YAG InnoSlab amplifier

We now characterize a second 1 µm laser operating at 100 MHz, with pulse energy of 1 mJ and wavelength of 1032 nm. The pulse length is of around 900 fs.

We scanned the delay stage in steps of 20 fs, over a range of 8 ps, corresponding to 400 points of delay with a step size of 3 µm.

Starting again with the autocorrelation, figure 14 shows the experimental data and the best Gaussian fit. The FWHM of the function is of 1497.5 fs. Applying the form factor for a Gaussian pulse, we get $1498/1.414 = 1059$ fs. This estimate fits in the order of magnitude that we expect the pulse width to be in.

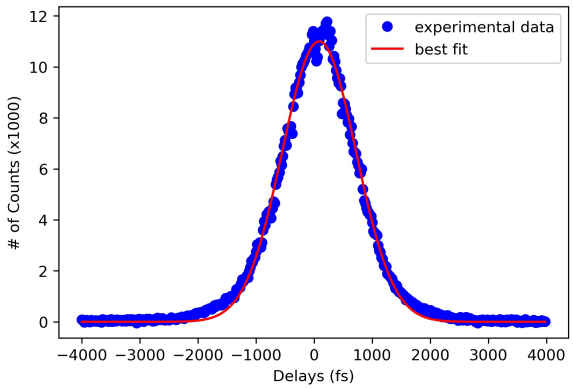

Figure 14: Gaussian fit of the amplifier autocorrelation

Applying once again 4.1 with a Gaussian TBWP, we obtain a pulse width of 517.05 fs, which is shorter than the 1059 fs we just found, so a pulse with these characteristics is indeed possible.

Again, we followed with the study of the credibility of the results in terms of the validity of the second harmonic. Figure 15 shows the overlap between the fundamental peak and the second harmonic with its frequencies doubled. Given the similarities between the two curves, it is indeed the second harmonic that is being retrieved with no cuts. The differences in peak centers shifts from this laser to the other are certainly due to the great difference in bandwidths between both lasers.

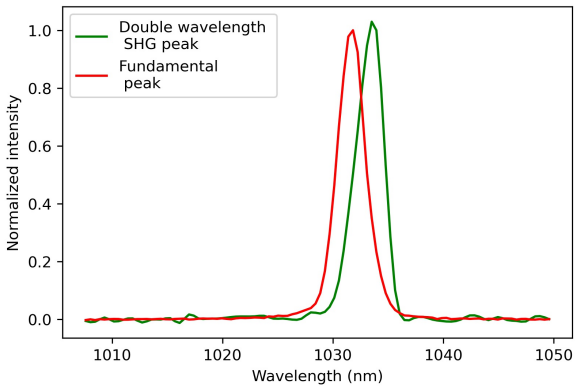

Figure 15: Plot of the amplifier spectrum of the fundamental pulse and of the second harmonic with its wavelength axis doubled.

Running through Femtosoft again, we find satisfactory results. Figure 17 shows the visual comparison of the original and retrieved FROG trace. As we can see, the original FROG trace is slightly less "Gaussian" than the previous one, with a slight tail on the upper part of the picture. The bulk of the pulse represented with the hotter colors (red/yellow) is very similar to the original one.

We thus reach a pulse width of 862.6 fs with a tiny error of 0.3%, well in accordance with what we expected it to be. This time however, it diverges more from the autocorrelation method by 22.8%. This can be explained by the shape of the pulse being less Gaussian as shown in Fig. 16. Indeed the TBWP differs from that of a Gaussian by a lot this time, standing at 1.123 in comparison with the Gaussians' 0.44.

Regarding the phase, a linear chirp can be observed, but again, we have to be skeptic about that.

We applied again the ptychographic algorithm, obtaining the results presented in figure 17. The retrieval was more successful than the previous with an error of 0.0623. This time, we were able to stretch the pulse a little more which explains the lower error.

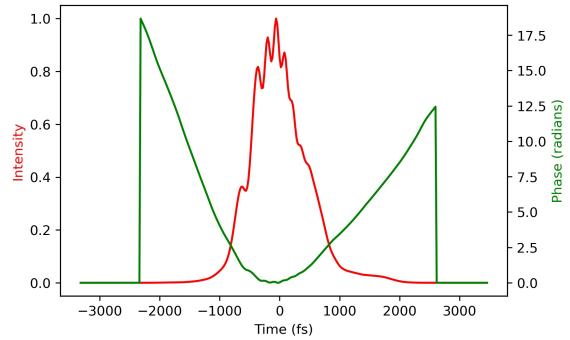

Figure 16: Retrieved amplifier pulse and phase using Femtosoft

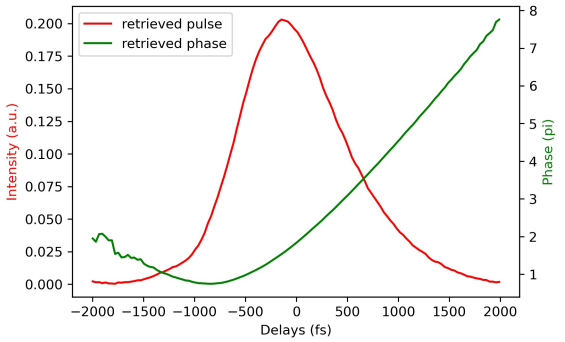

Figure 18: Ptychographic recovery of the amplifier pulse and phase

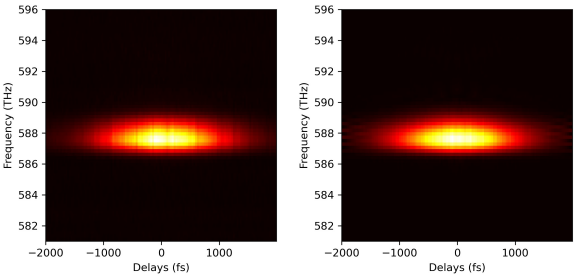

Figure 17: Original (left) and retrieved (right) amplifier FROG traces using the ptychographic algorithm

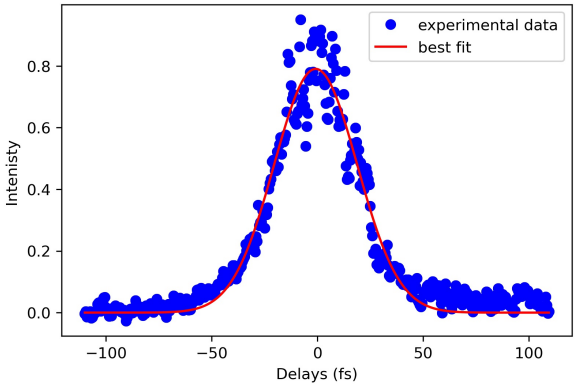

Figure 19: Gaussian fit of the Fastlite autocorrelation

Figure 18 shows the retrieved temporal pulse and phase and a recovered value of 875.9 fs. A Gaussian was fitted, but this time, it does not fit as well as in the previous example. The interval this value admits given the error is [821.3 , 930.5] fs, which includes the 862.6 fs previously found, and so we will take the previous value as the correct one.

Some linear chirp is observed here as the phase is parabolic for a section of the pulse. For the same reason than before, we deem this phase to be more trustworthy.

4.3. Fastlite mid-infrared OPCPA

We finally come to the laser that motivated this work. It operates at 100 MHz, with pulse energy of 60 µJ. The pulse length is of around 40 fs. The wavelength range is now in the mid-infrared at 3000 nm. We scanned the delay stage in steps of 0.5 fs, over a range of 220 ps, corresponding to 440 points of delay with a step size of 0.075 µm.

Figure 19 shows the the data retrieved, and the best Gaussian fit. The irregular data in peak hints that the pulse is not so well behaved, although it could also be due to some fluctuations in the air, temperature, humidity or illumination. Nevertheless, the FWHM of the fit is of 46 fs, and applying the Gaussian form factor, we retrieve $46/1.414 = 33$ fs. It is definitely in the range that we were expecting, and, in that sense, we can say the device worked properly. However we cannot evaluate by how much the measurement is off due to our uncertainty regarding the pulse shape. As we saw in the previous sections, this can alter the result by at least 22.8% for the case of the Amphos amplifier. This represents an interval between [24.2 ; 40.5] fs, which includes the 40 fs that we were anticipating. However, if the irregularities in the peak are not an error in the data acquisition, they suggests that the pulse might have several peaks, and, as such, the Gaussian does not go as high because it averages out all the values into one single peak. Should that be the case then the pulse is wider and fits more in the neighborhood of 40 fs. But this remains a highly qualitative analysis.

5. Conclusions

We have described in this work how we planned a frequency resolved optical gating diagnostic for the calculation of the temporal shape and spectral phase of a 3 µm mid-infrared laser. In particular, we tested a SHG-FROG recovery algorithm of ptychographic nature in the hope of achieving superior exactitude in the measurement.

We explored the difficulties of the characterization of pulses in this wavelength range and proposed a design optimized to tackle each of the difficulties. Specifically, we showed why the $AgGaS_2$ was the best choice for our application.

We detailed how the design evolved into the final product, and how the data acquisition was controlled.

We characterized, with great precision thanks to the FROG technique, two 1 µm lasers, the coherent mira Ti:sapphireoscillator and the amphos Yb:YAG InnoSlab amplifier, obtaining a pulse width of 188.2 fs for the first, and 862.6 fs for the latter. With less precision, we obtained a pulse width of 33 fs for the 3 µm fastlight mid-infrared OPCPA using the autocorrelation method.

To improve on this work, a spectrometer with a higher resolution could be used in order to avoid the stripe like traces for the 1 µm lasers. For a more precise characterization with FROG of the 3 µm pulse the photodiode can be replaced by a spectrometer.

Yet this is but the foundation on which future research in the Laboratory for Intense Lasers will be built on. We now have a greater confidence on the length of the pulse, which in turn allows for more meaningful research in the domain of ultrafast optics.

Acknowledgements

First and foremost I would like to express my sincerest gratitude to my supervisors. Thank you Prof. Gonçalo Figueira for the opportunity, and patience which made this thesis possible. Very special thanks particularly to Prof. Hugo Pires for his invaluable support and patience, and for always being so reachable. Thank you so much. Thank you also to Joana Alves for her help in the Laboratory for Intense Lasers, and to my colleague Gonçalo Vaz.

I would like to extand my thanks also to the faculty, Instituto Superior Técnico, for all its learning opportunities and especially, its lesson in perseverance.

References

[1] Saleh Bahaa E. A. and Malvin Carl Teich. Fundamentals of Photonics 3rd Edition. 5:1078–1159, 2013.

[2] Edwin J. Akutowicz. On the determination of the phase of a Fourier integral. I. *Transactions of the American Mathematical Society*, 1956.

[3] Edwin J. Akutowicz. On the Determination of the Phase of a Fourier Integral, II. *Proceedings of the American Mathematical Society*, 1957.

[4] Daniel J. Kane and Rick Trebino. Single-shot measurement of the intensity and phase of an arbitrary ultrashort pulse by using frequency-resolved optical gating. *Optics Letters, Vol. 18, Issue 10, pp. 823-825*, 18(10):823–825, may 1993.

[5] Rick Trebino. Frequency-Resolved Optical Gating: The Measurement of Ultrashort Laser Pulses. *Frequency-Resolved Optical Gating: The Measurement of Ultrashort Laser Pulses*, pages 1–88, 2000.

[6] Pavel Sidorenko, Oren Lahav, Zohar Avnat, and Oren Cohen. Ptychographic reconstruction algorithm for FROG: Supreme robustness and super-resolution. *2016 Conference on Lasers and Electro-Optics, CLEO 2016*, 3(12), 2016.

[7] P. K. Bates, O. Chalus, and J. Biegert. Ultrashort pulse characterization in the mid-infrared. *Optics Letters*, 35(9):1377, 2010.

[8] B. A. Richman, M. A. Krumbügel, and R. Trebino. Temporal characterization of mid-IR free-electron-laser pulses by frequency-resolved optical gating. *Optics Letters, Vol. 22, Issue 10, pp. 721-723*, 22(10):721–723, may 1997.

[9] J. Hunter, K. W. DeLong, Rick Trebino, and W. E. White. Frequency-resolved optical gating with the use of second-harmonic generation. *JOSA B, Vol. 11, Issue 11, pp. 2206-2215*, 11(11):2206–2215, nov 1994.

[10] Ivan Amat-Roldn, Iain G. Cormack, Pablo Loza-Alvarez, Emilio J. Gualda, and David Artigas. Ultrashort pulse characterisation with SHG collinear-FROG. *Optics Express*, 12(6):1169, 2004.

[11] R. Trebino, R. Jafari, S. A. Akturk, P. Bowlan, Z. Guang, P. Zhu, E. Escoto, and G. Steinmeyer. Highly reliable measurement of ultrashort laser pulses. *Journal of Applied Physics*, 128(17), 2020.